Characterization of the blue-light activated adenylyl cyclase mPAC by flash photolysis and FTIR spectroscopy

Silke Kerruth[1], Pit Langner[1], Sarah Raffelberg[2], Wolfgang Gärtner[3] und Joachim Heberle[1*]

[1]Freie Universität Berlin, Experimental Molecular Biophysics, Arnimallee 14, 14195 Berlin, Germany.

[2] University of Geneva, Department of Botany and Plant Biology, 30 Quai E. Ansermet, 1211 Geneva, Switzerland.

[3]Max Planck Institute for Chemical Energy Conversion, Stiftstr. 34-36, 45470 Mühlheim a. d. Ruhr, Germany.

*Corresponding author:

Tel: +49-30-838-56164

Fax: +49-30-838-56510

email: joachim.heberle@fu-berlin.de

KEYWORDS

flavoprotein, LOV, optogenetics, photoreceptor

29   **ABSTRACT**

30   The recently discovered photo-activated adenylyl cyclase (mPAC from *Microcoleus chthonoplastes)* is

31   the first PAC that owes a light-, oxygen- and voltage sensitive (LOV) domain for blue-light sensing.

32   The photoreaction of the mPAC receptor was studied by time-resolved UV/Vis and light-induced

33   Fourier-transform infrared (FTIR) absorption difference spectroscopy. The photocycle comprises of

34   the typical triplet state LOV_{715} and the thio-adduct state LOV_{390}. While the adduct state decays with a

35   time constant of 8 s, the lifetime of the triplet state is with 656 ns significantly shorter than in all other

36   reported LOV domains. The light-induced FTIR difference spectrum shows the typical bands of the

37   LOV_{390} and LOV_{450} intermediates. The negative S-H stretching vibration at 2573 cm^{-1} is asymmetric

38   suggesting two rotamer configurations of the protonated side chain of C197. A positive band at

39   3636 cm^{-1} is observed, which is assigned to an internal water molecule. In contrast to other LOV

40   domains, mPAC exhibits a second positive feature at 3674 cm^{-1} which is due to the O-H stretch of a

41   second intrinsic water molecule and the side chain of Y476. We conclude that the latter might is

42   involved in the dimerization of the cyclase domain which is crucial for ATP binding.

43

44

45

46

47

48

49

50

51

52

53

INTRODUCTION

Blue and ultraviolet light is the wavelength range with the highest energy of the sun's emission that reaches the surface of the earth. These light qualities are ambivalent for living organisms. They can be employed as high energy sources, but both blue and ultraviolet light can cause severe damage in tissue and in biological macromolecules such as DNA or proteins, in a direct manner or via generation of singlet oxygen and other ROS. Accordingly, nearly all organisms have developed proteins during evolution to detect this high energy light in order to adapt their lifestyle in response to irradiation intensity or duration. In many cases, these blue-light (BL) sensitive receptors use flavin derivatives as chromophores (1).

Besides many others, e.g., histidine kinases, DNA-binding motifs or phosphodiesterases, adenylyl cyclases were recently added to the broad variety of light-regulated signaling domains. Furthermore, the identification of flavoproteins carrying adenylyl cyclases (PAC) (2), opened a new drawer in the toolbox of optogenetics, as in particular cAMP and to a lesser extent cGMP are major players in many metabolic pathways. Schröder-Lang et al. (3) demonstrated in an *in vivo* experiment that the cellular level of the second messenger cAMP can be rapidly changed by light. The functional expression in various cells like oocytes from *Xenopus laevis* (3), bacteria, fruit flies and rodent neurons and their manipulation by light identified PACs as powerful optogenetic tools.

The receptors that mediate photophobic response in the unicellular flagellate *Euglena gracilis*, were named PACα and PACβ. These proteins comprise two flavin adenine dinucleotide (FAD) binding domains, F1 and F2, belonging to the family of BLUF (blue-light using FAD) domains, each of which being fused to a catalytic adenylyl cyclase (AC) domains, C1 and C2. These AC domains show homology to class III adenylyl cyclases and form intermolecular heterodimers with two putative substrate binding sites (4). Illumination with blue-light leads to a fast increase (within seconds (5, 3)) in cAMP level with an 80-fold higher cyclase activity in the light (2). A bacterial photo-activated adenylyl cyclase was found in *Beggiatoa* (6). bPAC consists of a single BLUF with a downstream AC domain. With 350 amino acids, it is of much smaller size than PAC from *Euglena*. bPAC shows a 300-fold increase in cyclase activity upon light activation and decays thermally within 13 s. Furthermore, it was shown that bPAC produces large inward currents when expressed parallel to

82   cAMP dependent channels in oocytes (6). Recently, a new form of photo-activated adenylyl cyclases

83   was found in *Microcoleus chthonoplastes* (7). This receptor, called mPAC, uses a LOV (light-,

84   oxygen- and voltage-sensitive) domain for blue-light sensing and shows comparable light sensitivity to

85   bPAC. Although the increase of activity under BL irradiation is only 30-fold, its overall higher

86   constitutive activity in the dark as well as in light reveals in much higher cAMP levels in cells and,

87   thus, to a better response (7).

88   LOV domains belong to the Per-ARNT-Sim (PAS) superfamily with its classical α,β fold, consisting

89   of a five-stranded anti-parallel β-sheet and four helices (8). Within this fold a flavin mononucleotide

90   (FMN) is non-covalently bound that acts as chromophore. Absorption of a blue photon by FMN of

91   ground state LOV, LOV_{445}, leads to the electronically excited state which decays within a few

92   nanoseconds via intersystem crossing to the triplet state, LOV_{715} (9). The triplet state decays

93   subsequently with a time constant of a few microseconds into the adduct state $LOV_{390,}$ most probably

94   via a neutral radical mechanism (10). This intermediate is characterized by a covalent bond that is

95   formed between the C(4a) of the isoallaxazine ring of the FMN and the terminal sulfur of a nearby

96   cysteine (11, 9). Due to strained protein conformation, adduct state decays thermally into the ground

97   state LOV_{445}. This decay strongly varies among the large family of LOV domains and covers the time

98   range from seconds to hours (12, 11, 13, 14).

99   Associated with the photo activity of the chromophore are structural changes of the apo-protein.

100   Fourier transform infrared (FTIR) spectroscopy is a powerful method to study structural changes and

101   was applied to several LOV proteins (15-22) in the past, to elucidate the signal transfer mechanism of

102   plant-type phototropins (20, 21) as well as of their bacterial analogues, like YtvA from *Bacillus*

103   *subtilis* (16). These studies agree well with previous NMR experiments (23) and demonstrate that the

104   J_α-helix, which is a conserved structural element linking the LOV and the kinase domain, unfolds in

105   full-length phototropin1 upon light absorption (21)*,* thereby activating the kinase domain. However,

106   the activation of the kinase domain is neither accompanied by protonation changes nor changes in the

107   strength of the hydrogen bond network of carboxylic side chains (21). Recent studies showed that

108   YtvA is a dimer independent on its activation state (24, 25). However, size exclusion chromatography

109   (SEC) and circular dichroism (CD) spectroscopy on aureochrome 1 demonstrated that dimerization of

110   the LOV domains upon light illumination (26, 22) leads to activation of the sensor domain (27).

111   Dimerization and structural changes like α-helical unfolding may also play a role in the signal transfer

112   of mPAC as its adenylyl cyclase domain can only react as a dimer. Whether this dimerization is

113   induced by the presence of the LOV domain has so far not been clarified.

114   In this study, we characterize the kinetic and structural properties of the recently discovered photo-

115   activated adenylyl cyclase mPAC. The UV/Vis absorption spectrum indicates a LOV1 like domain of

116   mPAC. Determination of kinetics of the decay of the triplet state identify a significant shorter life time

117   of about 650 ns in comparison to other LOV domains (typically about 2 µs), while the decay of the

118   adduct state is with about 8 s within the usual range. Furthermore, the steady state light-induced FTIR

119   difference spectroscopy provides molecular insight into the structural changes associated with the

120   conversion into the putative signaling state LOV_{390}.

121

122

123

124 **MATERIAL AND METHODS**

125 *Expression and Purification of wild-type mPAC and the Y476F variant*

126 Protein expression and purification was performed as described (7). Briefly, *E.coli* RP were grown in

127 dYT media. Expression was induced by 0.4 mM IPTG and maintained at 18 °C for 48 h at 400 rpm in

128 the dark. Cells were harvested by centrifugation at 5700xg for 25 min. The pellet was resuspended in

129 lysis buffer (100 mM Tris pH 8, 600 mM NaCl, 10 % Glycerol, 500 µM PMSF). Subsequently, cells

130 were disrupted by two passages through a valve with 1.7 bar (TS Series Benchtop, Costant System).

131 Centrifugation at 22000xg for 30 min then separated the cell debris from the soluble fraction. The

132 supernatant was subjected to affinity chromatography via a Ni-NTA column (about 3 ml) that was

133 equilibrated with lysis buffer. The column was washed with 10 ml each of the washing buffers A and

134 B (50 mM Tris pH 8, 200 mM NaCl, 5 % Glycerol, 10 mM (A) and 20 mM (B) imidazole), followed

135 by protein elution with 10 ml of elution buffer (50 mM Tris pH 8, 200 mM NaCl, 5 % Glycerol and

136 130 mM imidazole). After chromatography, 4 mM DTT was added to each fraction to avoid

137 aggregation of the protein. For a second purification step, the combined mPAC containing fractions

138 were loaded on SEC (Sephadex 25) column operated by an Äkta avant 25 (GE healthcare). Fractions

139 containing pure mPAC were concentrated and stored in a final buffer (50 mM Tris pH 8, 200 mM

140 NaCl, 5 % glycerol, 3 mM DTT).

141 Site-specific mutation was inserted by polymerase chain reaction (PCR) using the QuikChange®

142 manual (Stratagene). As primers were used GGA AAA GGG GAA ATG ATC AAC TTT TGG CTG

143 GTT GGG AAG CAG (forward) and CTG CTT CCC AAC CAG CCA AAA GTT GAT CAT TTC

144 CCC TTT TCC (backward). The purification was performed accordingly to the wt and with similar

145 yields.

146

147 *Flash photolysis experiments*

148 Purified mPAC was diluted to a concentration of 60 µM dissolved in 50 mM Tris pH 8, 200 mM

149 NaCl, 5 % Glycerol, 3 mM DTT). The sample was excited by a short pulse from a Nd:YAG driven

150 OPO laser system (pulse length at 475 nm was 10 ns, energy density of 2.5 mJ/cm^2, one pulse every

151 60 seconds). Flash photolysis experiments in the UV/Vis range were performed on two time scales:

152 the faster time range (<300 μs) was recorded with a Xe arc lamp as light source in pulsed mode and

153 the slower time scale (>30 μs) was detected with the lamp in continuous wave operation. Both traces

154 were averaged on a quasi-logarithmic time-scale and merged to yield time traces covering the time

155 range from 50 ns to 50 s. Ten kinetic traces were averaged at each selected wavelength.

156 For the kinetics in dependence of imidazole, an appropriate volume of concentrated imidazole solution

157 (8 M at pH 8) was added to the sample. After mixing, the fast and slow kinetics were recorded at 390

158 nm as just described.

159

160 *FTIR spectroscopy*

161 Light-induced FTIR difference spectroscopy was performed as previously described (15). Briefly, the

162 sample was transferred in 10 mM Tris pH 8, 100 mM NaCl, 1 mM DTT buffer and dried on a BaF_2

163 window by a gentle stream of dry air. The protein film was rehydrated with the saturated vapor phase

164 of a glycerol/water mixture (1:1 wt/wt). Sample hydration was sufficient, as deduced from the IR

165 absorption in the O-H stretching range (at around 3,300 cm^{-1}). Sample excitation was performed by the

166 same LED as for the UV/Vis experiments (see above). Infrared experiments were performed on a

167 Vertex 80v spectrometer (Bruker Optics, Ettlingen, Germany). FTIR difference spectra were

168 calculated by subtraction of the dark state spectra from the spectra recorded under photo stationary

169 conditions. Spectra were recorded at a spectral resolution of 4 cm^{-1} and represent the average of 2024

170 scans. Data analysis was performed with OriginPro 8.1G from Origin Lab, while fitting was done in

171 OPUS5.5 from Bruker Software.

172

173

174 **RESULTS**

175 *UV/Vis absorption spectroscopy*

176 The LOV domain of mPAC binds non-covalently flavin mononucleotide (FMN) as cofactor. FMN

177 shows a typical absorption spectrum in the blue around 450 nm with vibrational fine structure at 423

178 and 474 nm (Fig. 1). The absorption in the UVA region (315 to 400 nm) of protein-bound FMN is

179 strongly influenced by the amino acid surrounding as shown in recent studies (28). mPAC exhibits a

180 double peak in this region similar to the LOV1 domain of phototropin. The vibrational fine structure

181 becomes clearly visible after size-exclusion chromatography (grey trace in Fig. 1). Ni-NTA affinity

182 purification resulted in a sample with a ratio of 27.3 A_{280}/A_{450} nm (black trace). Size exclusion

183 chromatography significantly improved the purity as inferred from an A_{280}/A_{450} ratio of 10.3.

184 Considering the theoretical ratio of 7.6 for a fully assembled protein (7), the chromophore loading of

185 mPAC is about 70 % which agrees well with previously reported results (7).

186 Pulsed laser excitation of mPAC results in a photocycle with two distinctly different intermediates.

187 The triplet state is characterized by three absorption bands at 390, 660 and 715 nm. The kinetics of

188 formation and decay of the intermediates were followed at 20 °C (Fig. 2). Assuming single

189 exponential behavior, the triplet decays with time constants of 790±20 ns (660 nm) or 640±15 ns

190 (715 nm). As the absorption at 390 nm is also characteristic to the adduct state, the time trace at

191 390 nm reflects two clearly separated decays with time constants of 570±11 ns for LOV_{715} and

192 8.2±0.5 s for LOV_{390}. The latter decays directly into the initial ground state as inferred from the

193 identical time constant of 8.2±0.2 s for the recovery kinetics observed at 450 nm. It should be pointed

194 out here that the relatively long recovery time of mPAC is challenging for the ns flash photolysis

195 experiments as the repetition rate was one pulse per minute. Care was taken to avoid accumulation of

196 the photoproduct that might interfere with the analysis of the dark state by shading effects or

197 unintended photochemistry of the photoproduct. The differences in the decay of the triplet state

198 detected at different wavelengths are not significant. The average time constant is 656 (±81) ns.

199 It was reported for other LOV domains that the presence of imidazole accelerates the thermal decay of

200 the adduct state via a base-catalyzed mechanism (29). In this mechanism, imidazole acts as a base to

201 accept the proton from the N5 of the isoallaxazine ring of FMN as a prerequisite for bond cleavage in

202 the thio-adduct of FMN with the sulfhydryl of the reactive cysteine. In fact, also for mPAC the

203 influence of imidazole on the kinetics of the recovery of the ground state could be detected (Fig. 3).

204 While the decay of the triplet state is not influenced by the imidazole concentration, the decay of the

205 adduct state (= reformation of the parental state) is two-fold accelerated at concentrations of 500 mM.

206

207

208   *FTIR differences in the 1800-900 cm^{-1} region*

209   UV/Vis spectroscopy is an excellent tool to trace the electronic changes after light excitation of the

210   chromophore FMN. The succeeding structural changes including the apo-protein, however, are best

211   studied by FTIR spectroscopy. Light-induced differences are recorded under photo-stationary

212   conditions to reveal the molecular changes between the ground and the long-lived adduct state. The

213   resulting spectra in the region between 1800 and 900 cm^{-1} (Fig. 4) include the amide I and II region,

214   which is indicative to structural changes on the protein backbone, as well as the vibrations of most

215   amino acids side chains and the FMN chromophore. Like in other LOV domains, the FTIR difference

216   spectrum is dominated by the vibrational bands of the chromophore because the formation of the

217   adduct state induces a large change in the dipole moment of FMN, and as known from other LOV

218   domains, secondary structure changes of the protein are often of minor intensity. Bands of the adduct

219   state at 1726, 1688, 1655, 1625, 1541, 1520, 1427, 1367, 1331, 1304, 1190 and 1092 cm^{-1} (Fig. 4)

220   appear after blue-light excitation (positive absorbance), while bands at 1714, 1695, 1676, 1583, 1552,

221   1352, 1273, 1248, 1223 and 1082 cm^{-1} disappear (negative absorbance) and, thus, correspond to the

222   ground state. The band assignment is based on comparison to LOV1 from phototropin-1 from

223   *Chlamydomonas reinhardtii* (15). The region between 1800 and 1000 cm^{-1} provides additional

224   information when the spectra of mPAC in H_2O, D_2O and $H_2^{18}O$ are compared (see Fig. 4). The $H_2^{18}O$

225   exchange (Fig. 4, lower trace) yields a change in intensity of the band at 1655/1641 cm^{-1}, however, no

226   further significant changes were observed. In contrast, the D_2O exchange (Fig. 4, upper trace) shows

227   more drastic changes. In the LOV$_{390}$ intermediate several bands are shifted. One band in the amide I

228   region at 1655 cm^{-1} is shifted upwards to 1660 cm^{-1}, while another band at 1685 cm^{-1} is slightly

229   downshifted to 1683 cm^{-1}. Furthermore, the positive band at 1520 cm^{-1} disappears almost completely.

230   The positive bands at 1427, 1376, and 1304 cm^{-1} also disappear, similar as observed before for the

231   phot-LOV1 domain (15). The negative bands at 1273, 1248, and 1223 cm^{-1} underlie the strongest

232   changes confirming the assignment to potent indicators for hydrogen bond interactions (15), while the

233   negative band at 1082 cm^{-1} vanishes completely. In addition, the bands at 1352, 1131, and 1194 cm^{-1}

234   are shifted by a few wavenumbers.

235

236   *FTIR spectra in the S-H stretching region*

237   As the formation of the adduct state requires breakage of the sulfhydryl bond of the involved cysteine

238   residue, the S-H stretching vibration represents a local sensor of the structure surrounding the

239   chromophore. The light-dark difference spectrum of mPAC (Fig. 5) shows the typical negative band

240   recorded in all LOV domains. This band is assigned to cysteine 197 based on the homology to other

241   LOV domains. The frequency of the S-H stretching vibration is decreased in relation with an increase

242   in hydrogen donating character of the S-H moiety. mPAC shows a negative difference band at

243   2573 cm^{-1} identical to the LOV2 domain of phototropin-1 (16). The band displays a shoulder at the

244   lower frequency end which is fitted by a second band with a frequency of 2557 cm^{-1}. The same was

245   observed for the S-H stretching band of the homologous cysteine residue of YtvA and the LOV1

246   domain of phototropin with minima at 2569/2561 and 2570/2562 cm^{-1}, respectively (16). In contrast,

247   the S-H stretching vibration of aureochrome 1 is sharp at a minimum of 2563 cm^{-1} (redrawn from

248   (30)). The two side bands in LOV1 and YtvA correspond to the two possible rotamer configurations of

249   the respective cysteines (C57 in LOV1 and C62 in YtvA). The occupancy of the two rotamers was

250   determined to 70 and 30 % from the crystal structure of YtvA (27) and LOV1 (27, 31). In close

251   agreement, the band areas of the fitted Gaussians in the FTIR spectrum revealed a distribution of 63

252   and 37 % for YtvA and 74 and 26 % for LOV1 (16). Spectral analysis of the S-H stretching band of

253   mPAC revealed with 90 and 10 % only a minor contribution of the other rotamer. As an additional

254   observation the frequency of the shoulder is shifted by 4-5 cm^{-1} in comparison to other LOV domains.

255

256   *FTIR Spectra in the 3800-2800 cm^{-1} region*

257   This frequency range is typical for single bond stretches (predominantly O-H, N-H and C-H in

258   proteins). This amide A region is not only sensitive to changes of the protein conformation but also to

259   changes in the hydrogen-bonded network. In the LOV_{390} minus LOV_{450} difference spectra of phy3-

260   LOV2, aureochrome 1 and YtvA a positive band in the region from 3620 to 3640 cm^{-1} is observed that

261   was assigned to a weakly hydrogen bonded internal water molecule in close vicinity to the FMN (32).

262   Formation of adduct state breaks the hydrogen bond of the FMN to this nearby water molecule. Thus,

263   the frequency of the O-H stretching vibration shifts from lower to higher wavenumbers and appear as

264   a positive band in the spectrum. However, mPAC shows an additional positive band in this region at

265   3674 cm^{-1}. To clarify if this band belongs as well to an O-H stretching mode of a water molecule,

266   measurements in D_2O and $H_2^{18}O$ were performed. The resulting difference spectra of the bands

267   influenced by the exchange are shown in Fig. 7. The exchange of water by D_2O shifts the S-H

268   vibration from 2572 to 1870 cm^{-1} (S-D vibration). Furthermore the O-H stretching vibrations

269   occurring at around 3650 cm^{-1} are downshifted to around 2700 cm^{-1} along with a decrease in extinction

270   coefficient.

271   As expected, the S-H stretching vibration is not changed in $H_2^{18}O$ whereas the band at 3632 cm^{-1} is

272   downshifted by 10 cm^{-1} characteristic for the O-H stretching vibrational band of a water molecule after

273   $^{16}O/^{18}O$ exchange. The band at 3674 cm^{-1} splits into two upon $H_2^{18}O$ exchange, showing a band at

274   3663 cm^{-1} with a shoulder at 3674 cm^{-1}. This shows that the band at 3674 cm^{-1} is composed of two

275   overlapping O-H stretching vibrations, only one arising from an intrinsic water molecule. The

276   frequency of the other band is indicative for the phenolic side chain vibration of a tyrosine residue.

277   Due to the fact that this band appears in mPAC only, it is reasonable to assume that it arises from a

278   residue in the adenylyl cyclase domain. First, we generated a T318A variant because T318 is directly

279   involved in ATP binding by forming hydrogen bonds to the ribose. However, the FTIR difference

280   spectrum was exactly the same as for the wild type (data not shown). The sequence alignment using

281   PHYRE2 (33) showed a conserved tyrosine residue at the C-terminus of the cyclase domain (Fig. 8).

282   To gauge the putative role of this residue, we generated the Y476F mutant. The UV/Vis absorption

283   spectrum and kinetics of the Y476F variant are identical to the wild type (data not shown). The FTIR

284   spectra of the wild type and the variant are identical as well. However, if H_2O is replaced by $H_2^{18}O$ the

285   same shift for the water bands appear but the shoulder at 3674 cm^{-1} disappears (Fig. 9). This

286   experiment clearly assigns the band at 3674 cm^{-1} to the O-H stretching vibration of the phenolic side

287   chain of Y476.

288

289

290

DISCUSSION

The photoreaction of the new adenylyl cyclase mPAC from *Microcoleus chthonoplastes* was studied by molecular spectroscopy. The visible spectrum, which reveals a double band feature in the UVA region, shows that the LOV domain of mPAC is similar to LOV1 from phototropin (28, 34). This finding is reflected by lacking of the otherwise conserved residues T418 and N425 in *Avena sativa* phot-LOV2 (A162 and M169 in mPAC), involved in determination of the spectral feature in the UVA region.

Time-resolved flash photolysis recorded the kinetics of the triplet decay with a time constant of 656 ($\pm$81) ns as one of the fastest lifetimes for LOV domains. Only for phot-LOV1 from *Chlamydomonas reinhardtii,* a time constant of 800 ns for a parallel formed triplet state LOV_{715a} was reported (11). Usually, the decay of the triplet state is a few µs, like for phot1 LOV1 (4 µs), LOV2 (1.9 µs), YtvA (2 µs) and aureochrome 1 (1.4 µs) (11, 14, 13). The back reaction at 20 °C to the initial ground state was determined with a time constant of 8.2 s. This value is in the range of the previously reported lifetime of 16 s (7).

The decay of the adduct state requires breakage of the S-C(4a) bond and proton transfer from N(5). For other studied LOV domains this reaction can be accelerated by a base-catalyzed mechanism employing imidazole (29). However, mPAC does not show significant changes in the kinetics of the dark state recovery in the presence or absence of imidazole, except for very high imidazole concentrations of 500 mM and 1 M the time constant increases to 4.5 and 2.1 s, respectively. This corresponds to a 2-fold and 4-fold acceleration. However, other LOV domains like aureochrome 1 from the Diatom *Phaeodactylum tricornutum* already show a 20-fold acceleration of ground-state recovery at imidazole concentrations of 1 mM (22) and a 30-fold increase was observed at 50 mM imidazole for LOV2 domain of *Avena sativa* phototropin-1 (29). Recent studies pointed out the importance of a threonine residue close to the FMN binding pocket in some fungal and bacterial LOV proteins (T101 in ENV1 and T27 in McLOVr) in the recruitment and dynamics of internal water molecules (35, 36). In mPAC, however, this residue is replaced by the hydrophobic valine, like in several other LOV domains. Furthermore the role of this threonine is quite diverted because mutation into isoleucine made the binding pocket of ENV1 less accessible for solvent molecules while the same

319   mutation in McLOV lead to an increase in the solvent-accessibility factor and made the adduct decay

320   sensitive to imidazole. Our finding that the adduct decay of mPAC is insensitive to low imidazole

321   concentration (up to 100 mM) shows that its LOV domain is more similar to that of ENV1 T101I with

322   an ordered structure regardless of water occupancy (35).

323   The light-induced FTIR difference spectrum demonstrates the high similarity of the mPAC domain to

324   other LOV domains. The spectrum shares the typical FMN bands and also reveals the expected shifts

325   due to H/D exchange. The difference bands in the amide I region around 1650 cm^{-1} are quite small in

326   comparison to other LOV domains like aureochrome 1. Thus, minor structural changes due to light

327   activation are considered. For further investigation of the reaction mechanism, size exclusion

328   chromatography measurements are future tasks.

329   The S-H stretching region also reveals the typical negative peak indicative for the disappearance of

330   sulfhydryl group, which we assigned to C197. This peak is asymmetric and can be fitted by two

331   Gaussians resulting with peaks at 2557 and 2573 cm^{-1}. The relative area of the two vibrational bands is

332   12 and 88 %. Thus, two rotamers of the reactive cysteine are present in mPAC as was also found in

333   other LOV domains (11, 16). In contrast to LOV1 from phototropin, the kinetics of the triplet state

334   decay is mono-exponential and does not provide any evidence for a second species.

335   A positive band at 3632 cm^{-1} is found in the water and amide A region for mPAC that is assigned to an

336   intrinsic water molecule analogous to other LOV domains (32). However, an additional positive band

337   was identified at 3674 cm^{-1} which is unique for mPAC. Tentatively been assigned to an alcoholic side

338   chain, the mutation of tyrosine 476 (Y476F) clearly proved that this band is composed by two

339   overlapping bands, one from another intrinsic water molecule and the other part arising from the

340   phenolic O-H stretch of Y476. Sequence alignment of the mPAC adenylyl cyclase domain with others

341   shows that the tyrosine residue is conserved in most of the domains or it is conservatively replaced by

342   a phenylalanine. This conservation explains the fully functional variant Y476F and underpins the

343   relevance of this residue. The structure of the adenylyl cyclase domain of mPAC was modeled using

344   SWISS-MODEL (37)(38) and the crystal structure of CyaC (PDB entry: 1WC5) as a template.

345   However, the resulting model didn't give insights into the position and function of Y467 because it

346   wasn't included in the model. Using PHYRE2 (33) as a modeling tool resulted in a very similar

347 structure as obtained from SWISS-MODEL but showed the C-terminus as an extension of two sheets

348 to the core β-sheet. Y476 is located in this β-sheet facing the α-helix that contains the conserved

349 residues N429 and R433 facing the dimer interface and involved in ATP binding (α-phosphate and

350 ribose) (37). In the model, the distance (9.4 Å) is too far to form a hydrogen bond but the cavity in

351 between these residues seems sufficiently large to accommodate one (or more) water molecule(s). This

352 structure could explain the second water molecule that was observed in the FTIR difference spectra.

353 However, this models can provide only a very coarse view. To further investigate the importance of

354 this tyrosine residue, experimental techniques that are sensitive to the oligomeric state in the light and

355 dark as well as activity assays need to be applied (39).

356 The LOV domain of mPAC from *Microcoleus chthonoplastes* exhibits most features identified also in

357 other LOV domains with steady-state (32, 40, 16, 41, 42, 30, 43) and time-resolved spectroscopy (20,

358 44). The remarkably rapid triplet decay, so far the fastest observed ever in LOV domains, must be

359 ascribed to the protein pocket which destabilizes the triplet state of the flavin chromophore. This

360 suggestion is based on the rationale that the rate of triplet decay is controlled by the accessibility to

361 molecular oxygen which quenches the triplet state (destabilization). The finding that the overall

362 changes between the dark and the lit state are marginal is not surprising as it was already determined

363 for many LOV domains that light-induced conformational changes are small, and the signal travels

364 mostly through a rearrangement of hydrogen bonds, induced by rotation of asparagine and glutamine

365 side chains (21, 42). Even changes in the AC domain must not be considered large, as the activation

366 mechanism might not include large secondary structural changes, but instead a rearrangement of two

367 AC moieties relative to each other, as it is known that the active site of ACs is formed at the interface

368 of two monomers (42).

369 The finding of a LOV domain (instead of the BLUF domains described so far for PAC) as the light-

370 regulating domain seemed at first glance advantageous, as many LOV domains show a stable

371 photoproduct state, i.e., a retarded recovery of the parental state, a property advantageous for

372 optogenetic applications. In mPAC, however, the decay of the photoproduct is fairly fast, requiring

373 similarly as in the BLUF domain regulated ACs, intense exposure of the cells or tissue to blue light.

374 Extended mutagenesis studies in relation to sequence alignments might help identifying amino acids

375　that stabilize the photoproduct state without interfering with the communication between the LOV and

376　the AC domain.

377

378

379　**ACKNOWLEDGMENT**

382

383

384　**REFERENCES**

385

386　1. Losi, A. and W. Gärtner (2012) The evolution of flavin-binding photoreceptors: an ancient
387　　　chromophore serving trendy blue-light sensors. *Annu. Rev. Plant Biol.* **63,** 49-72.
388　2. Iseki, M., S. Matsunaga, A. Murakami, K. Ohno, K. Shiga, K. Yoshida, M. Sugai, T. Takahashi, T. Hori
389　　　and M. Watanabe (2002) A blue-light-activated adenylyl cyclase mediates photoavoidance in
390　　　Euglena gracilis. *Nature* **415,** 1047-1051.
391　3. Schröder-Lang, S., M. Schwärzel, R. Seifert, T. Strünker, S. Kateriya, J. Looser, M. Watanabe, U. B.
392　　　Kaupp, P. Hegemann and G. Nagel (2007) Fast manipulation of cellular cAMP level by light in
393　　　vivo. *Nat Methods* **4,** 39-42.
394　4. Looser, J., S. Schröder-Lang, P. Hegemann and G. Nagel (2009) Mechanistic insights in light-induced
395　　　cAMP production by photoactivated adenylyl cyclase alpha (PACalpha). *Biol Chem* **390,** 1105-
396　　　1111.
397　5. Yoshikawa, S., T. Suzuki, M. Watanabe and M. Iseki (2005) Kinetic analysis of the activation of
398　　　photoactivated adenylyl cyclase (PAC), a blue-light receptor for photomovements of Euglena.
399　　　*Photochem Photobiol Sci* **4,** 727-731.
400　6. Stierl, M., P. Stumpf, D. Udwari, R. Gueta, R. Hagedorn, A. Losi, W. Gärtner, L. Petereit, M. Efetova,
401　　　M. Schwarzel, T. G. Oertner, G. Nagel and P. Hegemann (2011) Light modulation of cellular
402　　　cAMP by a small bacterial photoactivated adenylyl cyclase, bPAC, of the soil bacterium
403　　　Beggiatoa. *J Biol Chem* **286,** 1181-1188.
404　7. Raffelberg, S., L. Wang, S. Gao, A. Losi, W. Gärtner and G. Nagel (2013) A LOV-domain-mediated
405　　　blue-light-activated adenylate (adenylyl) cyclase from the cyanobacterium Microcoleus
406　　　chthonoplastes PCC 7420. *Biochem J* **455,** 359-365.
407　8. Taylor, B. L. and I. B. Zhulin (1999) PAS domains: Internal sensors of oxygen, redox potential, and
408　　　light. *Microbiol.Mol.Biol.Rev.* **63,** 479-506.
409　9. Swartz, T. E., S. B. Corchnoy, J. M. Christie, J. W. Lewis, I. Szundi, W. R. Briggs and R. A. Bogomolni
410　　　(2001) The photocycle of a flavin-binding domain of the blue light photoreceptor
411　　　phototropin. *J Biol.Chem.* **276,** 36493-36500.
412　10. Bauer, C., C. R. Rabl, J. Heberle and T. Kottke (2011) Indication for a radical intermediate
413　　　preceding the signaling state in the LOV domain photocycle. *Photochem Photobiol* **87,** 548-
414　　　553.
415　11. Kottke, T., J. Heberle, D. Hehn, B. Dick and P. Hegemann (2003) Phot-LOV1: Photocycle of a Blue-
416　　　Light Receptor Domain from the Green Alga Chlamydomonas reinhardtii *Biophys J* **84,** 1192-
417　　　1201.

418 12. Christie, J. M., M. Salomon, K. Nozue, M. Wada and W. R. Briggs (1999) LOV (light, oxygen, or
419   voltage) domains of the blue-light photoreceptor phototropin (nph1): binding sites for the
420   chromophore flavin mononucleotide. *Proc Natl Acad Sci U S A* **96,** 8779-8783.
421 13. Losi, A., B. Quest and W. Gärtner (2003) Listening to the blue: the time-resolved thermodynamics
422   of the bacterial blue-light receptor YtvA and its isolated LOV domain. *Photochem Photobiol*
423   *Sci* **2,** 759-766.
424 14. Nakasone, Y., T. Eitoku, D. Matsuoka, S. Tokutomi and M. Terazima (2006) Kinetic measurement
425   of transient dimerization and dissociation reactions of Arabidopsis phototropin 1 LOV2
426   domain. *Biophys J* **91,** 645-653.
427 15. Ataka, K., P. Hegemann and J. Heberle (2003) Vibrational Spectroscopy of an Algal Phot-LOV1
428   Domain Probes the Molecular Changes Associated with Blue-Light Reception. *Biophysical*
429   *Journal* **84,** 466-474.
430 16. Bednarz, T., A. Losi, W. Gartner, P. Hegemann and J. Heberle (2004) Functional variations among
431   LOV domains as revealed by FT-IR difference spectroscopy. *Photochem Photobiol Sci* **3,** 575-
432   579.
433 17. Sato, Y., T. Iwata, S. Tokutomi and H. Kandori (2005) Reactive cysteine is protonated in the triplet
434   excited state of the LOV2 domain in Adiantum phytochrome3. *J.Am.Chem.Soc.* **127,** 1088-
435   1089.
436 18. Iwata, T., D. Nozaki, Y. Sato, K. Sato, Y. Nishina, K. Shiga, S. Tokutomi and H. Kandori (2006)
437   Identification of the C=O Stretching Vibrations of FMN and Peptide Backbone by (13)C-
438   Labeling of the LOV2 Domain of Adiantum Phytochrome3. *Biochemistry* **45,** 15384-15391.
439 19. Kikuchi, S., M. Unno, K. Zikihara, S. Tokutomi and S. Yamauchi (2009) Vibrational assignment of
440   the flavin-cysteinyl adduct in a signaling state of the LOV domain in FKF1. *J Phys Chem B* **113,**
441   2913-2921.
442 20. Pfeifer, A., T. Majerus, K. Zikihara, D. Matsuoka, S. Tokutomi, J. Heberle and T. Kottke (2009)
443   Time-resolved Fourier transform infrared study on photoadduct formation and secondary
444   structural changes within the phototropin LOV domain. *Biophys. J.* **96,** 1462-1470.
445 21. Pfeifer, A., T. Mathes, Y. Lu, P. Hegemann and T. Kottke (2010) Blue light induces global and
446   localized conformational changes in the kinase domain of full-length phototropin.
447   *Biochemistry* **49,** 1024-1032.
448 22. Herman, E., M. Sachse, P. G. Kroth and T. Kottke (2013) Blue-Light-Induced Unfolding of the Jα
449   Helix Allows for the Dimerization of Aureochrome-LOV from the Diatom Phaeodactylum
450   tricornutum. *Biochemistry* **52,** 3094-3101.
451 23. Harper, S. M., L. C. Neil and K. H. Gardner (2003) Structural basis of a phototropin light switch.
452   *Science* **301,** 1541-1544.
453 24. Lee, R., J. Gam, J. Moon, S. G. Lee, Y. G. Suh, B. J. Lee and J. Lee (2015) A critical element of the
454   light-induced quaternary structural changes in YtvA-LOV. *Protein Sci* **24,** 1997-2007.
455 25. Jurk, M., M. Dorn, A. Kikhney, D. Svergun, W. Gartner and P. Schmieder (2010) The switch that
456   does not flip: the blue-light receptor YtvA from Bacillus subtilis adopts an elongated dimer
457   conformation independent of the activation state as revealed by a combined AUC and SAXS
458   study. *J Mol Biol* **403,** 78-87.
459 26. Buttani, V., A. Losi, T. Eggert, U. Krauss, K. E. Jaeger, Z. Cao and W. Gartner (2007) Conformational
460   analysis of the blue-light sensing protein YtvA reveals a competitive interface for LOV-LOV
461   dimerization and interdomain interactions. *Photochem Photobiol Sci* **6,** 41-49.
462 27. Moglich, A. and K. Moffat (2007) Structural basis for light-dependent signaling in the dimeric LOV
463   domain of the photosensor YtvA. *Journal.Of.Molecular.Biology.* **373,** 112-126.
464 28. Raffelberg, S., A. Gutt, W. Gärtner, C. Mandalari, S. Abbruzzetti, C. Viappiani and A. Losi (2013)
465   The amino acids surrounding the flavin 7a-methyl group determine the UVA spectral features
466   of a LOV protein. *Biol Chem* **394,** 1517-1528.
467 29. Alexandre, M. T., J. C. Arents, R. van Grondelle, K. J. Hellingwerf and J. T. Kennis (2007) A base-
468   catalyzed mechanism for dark state recovery in the Avena sativa phototropin-1 LOV2
469   domain. *Biochemistry* **46,** 3129-3137.

470   30. Kerruth, S., K. Ataka, D. Frey, I. Schlichting and J. Heberle (2014) Aureochrome 1 illuminated:
471   structural changes of a transcription factor probed by molecular spectroscopy. *Plos One* **9,**
472   e103307.
473   31. Fedorov, R., I. Schlichting, E. Hartmann, T. Domratcheva, M. Fuhrmann and P. Hegemann (2003)
474   Crystal Structures and Molecular Mechanism of a Light-Induced Signaling Switch: The Phot-
475   LOV1 Domain from Chlamydomonas reinhardtii *Biophysical Journal* **84,** 2474-2482.
476   32. Iwata, T., D. Nozaki, S. Tokutomi, T. Kagawa, M. Wada and H. Kandori (2003) Light-induced
477   structural changes in the LOV2 domain of Adiantum phytochrome3 studied by low-
478   temperature FTIR and UV-visible spectroscopy. *Biochemistry* **42,** 8183-8191.
479   33. Kelley, L. A., S. Mezulis, C. M. Yates, M. N. Wass and M. J. Sternberg (2015) The Phyre2 web portal
480   for protein modeling, prediction and analysis. *Nat Protoc* **10,** 845-858.
481   34. Salomon, M., J. M. Christie, E. Knieb, U. Lempert and W. R. Briggs (2000) Photochemical and
482   mutational analysis of the FMN-binding domains of the plant blue light receptor,
483   phototropin. *Biochemistry* **39,** 9401-9410.
484   35. Lokhandwala, J., Y. d. l. V. R. I. Silverman, H. C. Hopkins, C. W. Britton, A. Rodriguez-Iglesias, R.
485   Bogomolni, M. Schmoll and B. D. Zoltowski (2016) A Native Threonine Coordinates Ordered
486   Water to Tune Light-Oxygen-Voltage (LOV) Domain Photocycle Kinetics and Osmotic Stress
487   Signaling in Trichoderma reesei ENVOY. *J Biol Chem* **291,** 14839-14850.
488   36. El-Arab, K. K., A. Pudasaini and B. D. Zoltowski (2015) Short LOV Proteins in Methylocystis Reveal
489   Insight into LOV Domain Photocycle Mechanisms. *Plos One* **10,** e0124874.
490   37. Bordoli, L., F. Kiefer, K. Arnold, P. Benkert, J. Battey and T. Schwede (2009) Protein structure
491   homology modeling using SWISS-MODEL workspace. *Nat Protoc* **4,** 1-13.
492   38. Biasini, M., S. Bienert, A. Waterhouse, K. Arnold, G. Studer, T. Schmidt, F. Kiefer, T. Gallo
493   Cassarino, M. Bertoni, L. Bordoli and T. Schwede (2014) SWISS-MODEL: modelling protein
494   tertiary and quaternary structure using evolutionary information. *Nucleic Acids Res* **42,**
495   W252-258.
496   39. Liu, Y., A. E. Ruoho, V. D. Rao and J. H. Hurley (1997) Catalytic mechanism of the adenylyl and
497   guanylyl cyclases: modeling and mutational analysis. *Proc Natl Acad Sci U S A* **94,** 13414-
498   13419.
499   40. Ataka, K., P. Hegemann and J. Heberle (2003) Vibrational spectroscopy of an algal Phot-LOV1
500   domain probes the molecular changes associated with blue-light reception. *Biophys. J.* **84,**
501   466-474.
502   41. Iwata, T., D. Nozaki, S. Tokutomi and H. Kandori (2005) Comparative investigation of the LOV1
503   and LOV2 domains in Adiantum phytochrome3. *Biochemistry* **44,** 7427-7434.
504   42. Herman, E., M. Sachse, P. G. Kroth and T. Kottke (2013) Blue-Light-Induced Unfolding of the J
505   alpha Helix Allows for the Dimerization of Aureochrome-LOV from the Diatom
506   Phaeodactylum tricornutum. *Biochemistry* **52,** 3094-3101.
507   43. Herman, E. and T. Kottke (2015) Allosterically Regulated Unfolding of the A 'alpha Helix Exposes
508   the Dimerization Site of the Blue-Light-Sensing Aureochrome-LOV Domain. *Biochemistry* **54,**
509   1484-1492.
510   44. Thöing, C., A. Pfeifer, S. Kakorin and T. Kottke (2013) Protonated triplet-excited flavin resolved by
511   step-scan FTIR spectroscopy: implications for photosensory LOV domains. *Physical Chemistry*
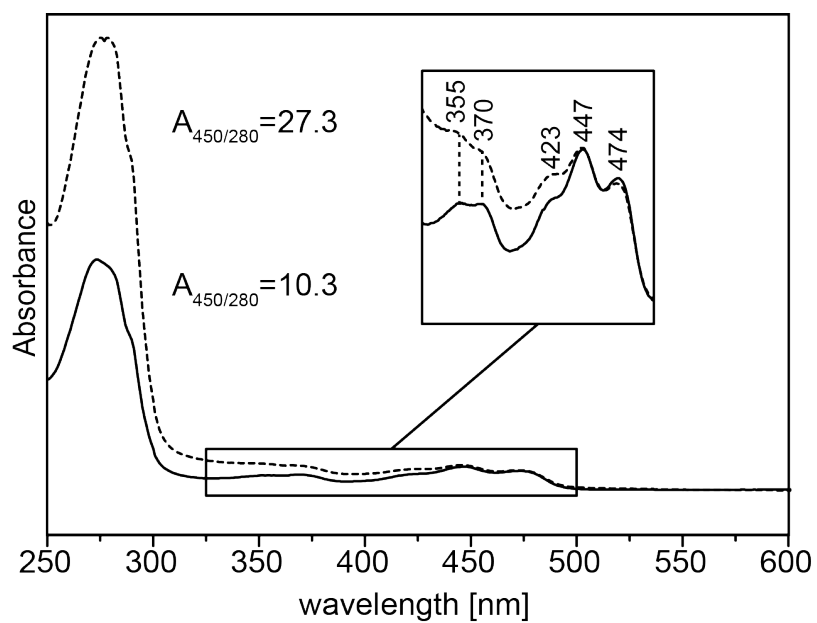512   *Chemical Physics* **15,** 5916-5926.
513
514
515
516
517

518

519
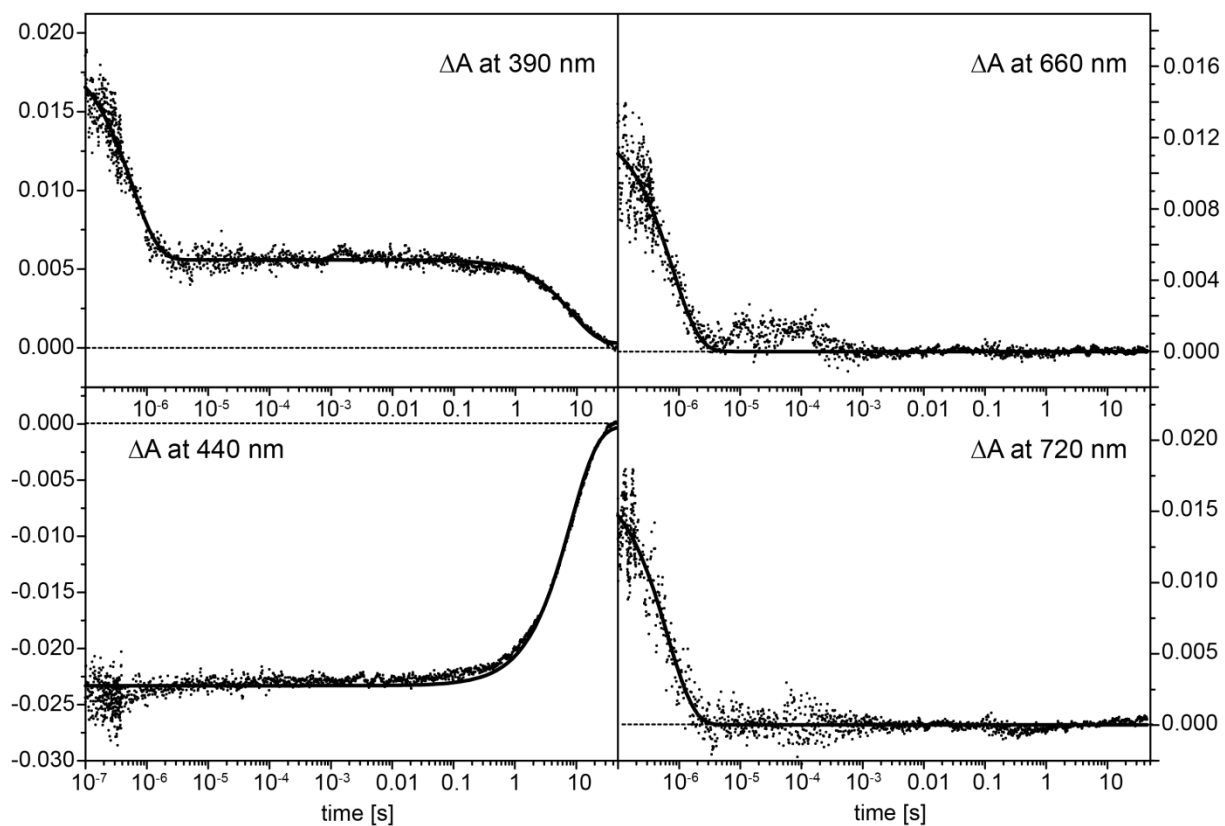
520

521

522

523

525

526

527   Figure 1: UV/Vis absorption spectra of mPAC before (dotted line) and after (black line) size exclusion

528   chromatography. The area between 325 and 500 nm is show as a zoom in (insert). The peaks of the

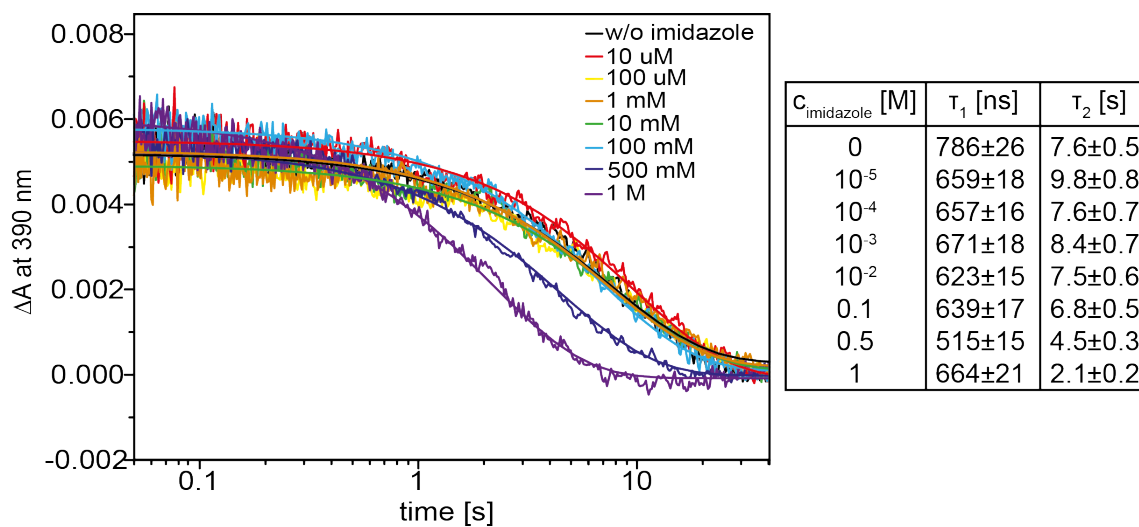529   blue and UVB absorption of the FMN chromophore are labeled.

530

531

532

Figure 2: Time-resolved UV/vis absorption difference spectroscopy of mPAC at 390, 440, 660 and 720 nm. The data points were fitted to single exponential decays for 440, 660 and 720 nm and with two exponential decays for 390 nm (black lines). The resulting time constants for the triplet decay are 570±11, 790±20 and 640±15 ns for 390, 660 and 720 nm, respectively. The differences in the time constants are not significant, leading to an average decay time of 656 (±81) ns. The time constants for the decay of the adduct state and the recovery of the ground state were determined to be 8.2±0.5 s and 8.2±0.2 s, respectively.

541

542

| $c_{imidazole}$ [M]	τ_1 [ns]	τ_2 [s]
0	786±26	7.6±0.5
10^{-5}	659±18	9.8±0.8
10^{-4}	657±16	7.6±0.7
10^{-3}	671±18	8.4±0.7
10^{-2}	623±15	7.5±0.6
0.1	639±17	6.8±0.5
0.5	515±15	4.5±0.3
1	664±21	2.1±0.2

543

544 Figure 3: Time-resolved UV/Vis difference spectra at 390 nm of mPAC at different imidazole

545 concentrations. The figures shows the slow time domain between 500 ms and 50 s corresponding to

546 the decay of the adduct state. The decay of the triplet state that occurs in the µs time domain is

547 included in the two-exponential decay fit of the data but not shown in the time trace. The

548 corresponding time constants τ_1 and τ_2 for the triplet and adduct state, respectively, are listed in the
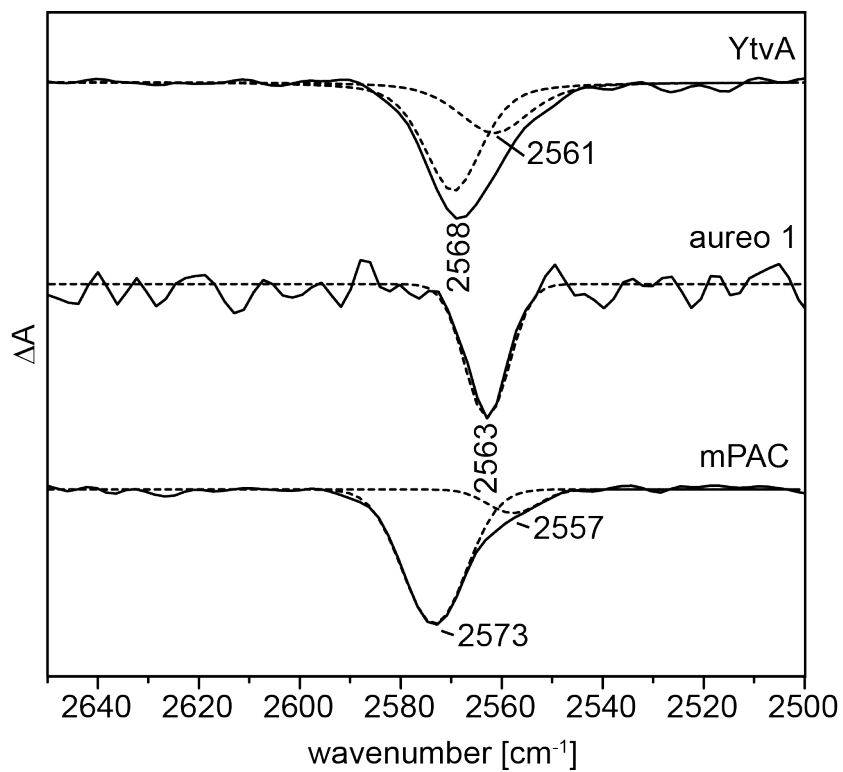
549 table on the right.

550

551

552
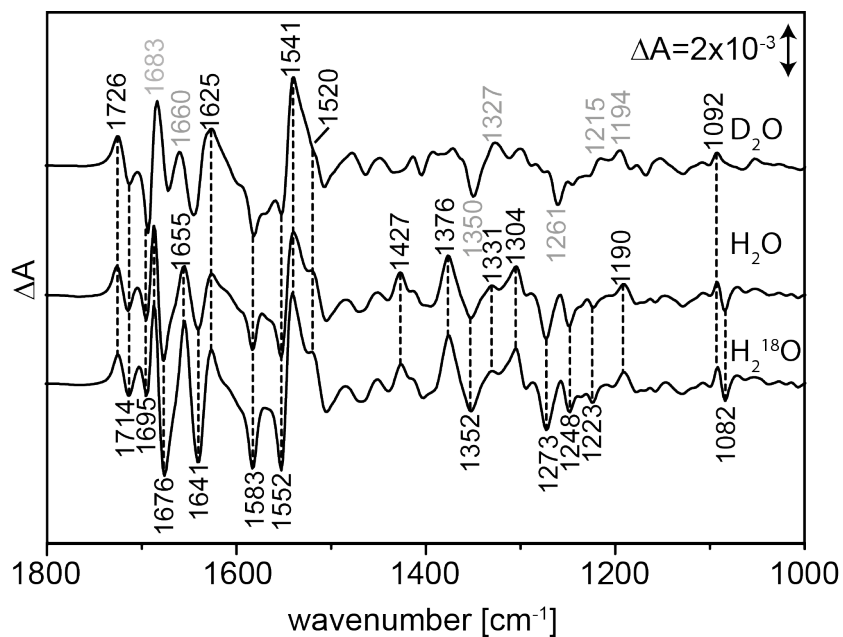
Figure 4: FTIR steady state difference spectra of mPAC with different isotope (^{2}H, ^{18}O) labeled water preparations. Similar bands in the spectra are connected with dotted lines, whereas those that differ between the spectra are labeled with corresponding wavenumbers colored in grey.
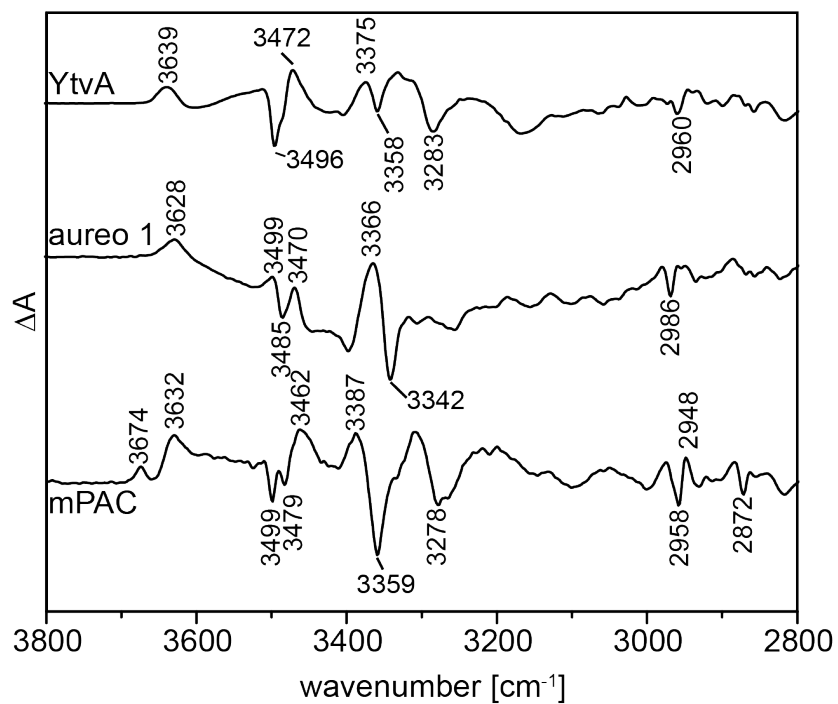
562 Figure 5: FTIR difference spectra of different LOV proteins in the S-H stretching region. The spectra

563 of aureochrome 1 and YtvA are replotted from refs. (30) and (16), respectively. The dotted lines are

564 Gaussian fits to the peaks. The peak of mPAC is fitted with two Gaussian functions with minima at
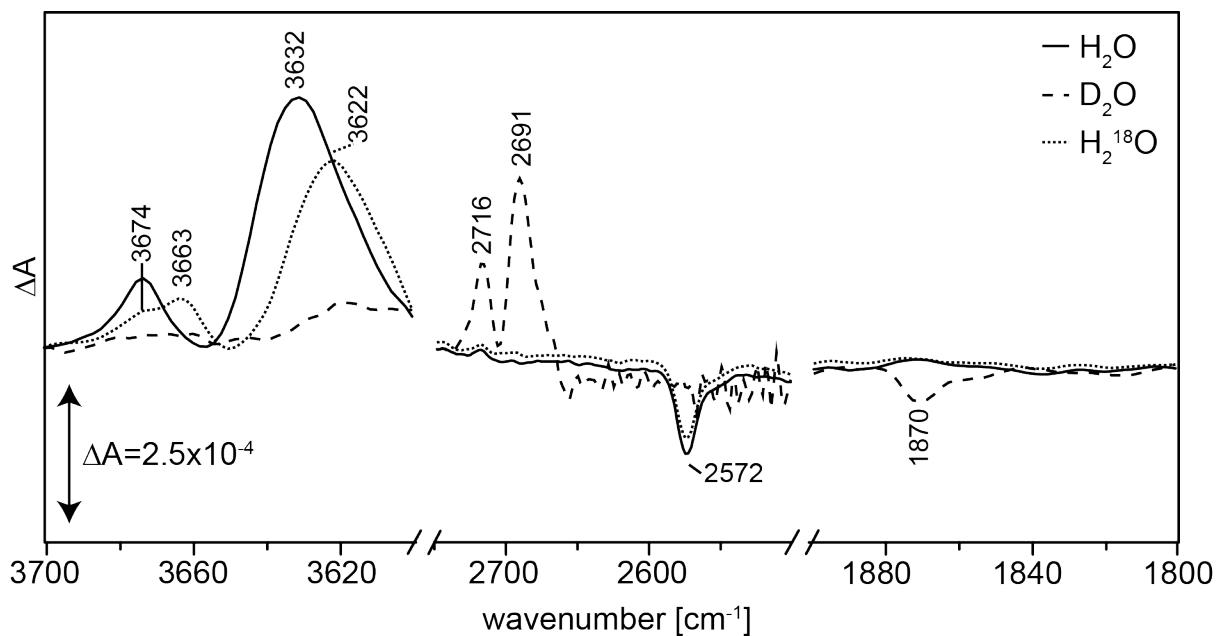
565 2573 and 2557 cm^{-1}.

567

568

569

Figure 6: Light-dark FTIR difference spectra of three different LOV proteins in the 2800-3800 cm^{-1} region. The upper spectrum corresponds to YtvA (replotted from (16)), the middle one to aureochrome 1 (30) and the lower one to mPAC. The numbers indicate the band positions in cm^{-1}.
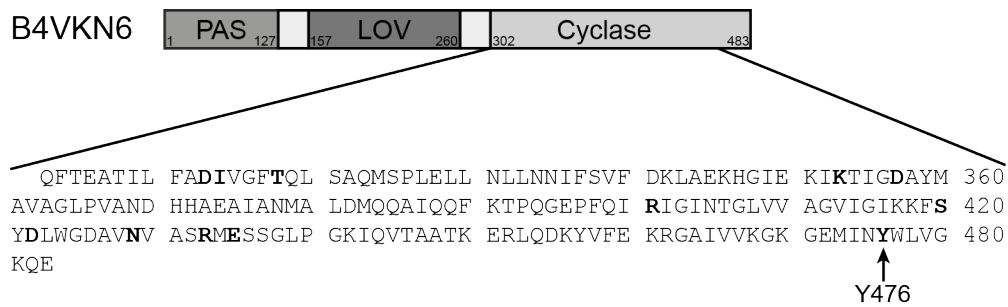
574

575

576

577

578 Figure 7: FTIR steady state difference spectra of mPAC with different isotope labeled water

579 preparations. The regions typical for dangling waters (3600-3700 cm^{-1}), for S-H vibrations (2750-

580 2500 cm^{-1}) and for S-D vibrations (1900-1800) are shown. The solid black line represents the mPAC

581 difference spectrum in H_2O, while the dotted line corresponds to the spectrum in $H_2^{18}O$ and the solid

582 grey line corresponds to the one in D_2O.

583

584

585


```
         QFTEATIL FADIVGFTQL SAQMSPLELL NLLNNIFSVF DKLAEKHGIE KIKTIGDAYM 360
AVAGLPVAND HHAEAIANMA LDMQQAIQQF KTPQGEPFQI RIGINTGLVV AGVIGIKKFS 420
YDLWGDAVNV ASRMESSGLP GKIQVTAATK ERLQDKYVFE KRGAIVVKGK GEMINYWLVG 480
KQE
```
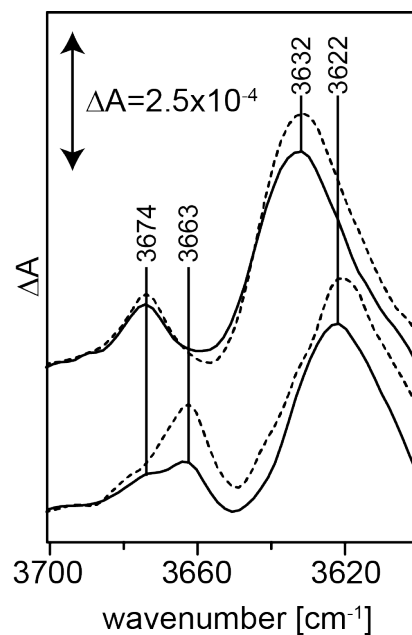Y476

586

587 Figure 8: Schematic view of the three domains of mPAC (B4VKN6) with the detailed sequence of the

588 adenylyl cyclase domain. The residues shown in bold are involved in ATP and ion binding

589 (Mg^{2+}/Ca^{2+}). The crucial residue Y467 is indicated by an arrow.

590

591

592

593 Figure 9: FTIR difference spectra of mPAC wild type (black line) and Y476F variant (red line) in H_2O

594 (upper spectra) and $H_2{}^{18}O$ (lower spectra) in the region between 3750 and 3600 cm^{-1}. Spectra have

595 been scaled to yield identical intensities of the S-H stretching vibration at 2572 cm^{-1}.

596